



**A 1,2,3-Dithiazolyl-*o*-naphthoquinone: A Neutral Radical  
with Isolable Cation and Anion Oxidation States**

Journal:	<i>Dalton Transactions</i>
Manuscript ID	DT-ART-03-2016-001249.R1
Article Type:	Paper
Date Submitted by the Author:	28-Apr-2016
Complete List of Authors:	Smithson, Chad; University of Guelph, Department of Chemistry MacDonald, Daniel; University of Guelph, Department of Chemistry Letvenuk, T.; University of Guelph, Department of Chemistry Carello, Christian; University of Guelph, Department of Chemistry Jennings, Michael; University of Western Ontario, Chemistry Lough, Alan; University of Toronto, Chemistry Britten, James; McMaster University, Department of Chemistry Decken, Andreas; University of New Brunswick, Chemistry Preuss, Kathryn; University of Guelph, Department of Chemistry



Journal Name

ARTICLE

## A 1,2,3-Dithiazolyl-*o*-naphthoquinone: A Neutral Radical with Isolable Cation and Anion Oxidation States

Received 00th January 20xx,  
Accepted 00th January 20xx

DOI: 10.1039/x0xx00000x

www.rsc.org/

Chad S. Smithson,<sup>a</sup> Daniel J. MacDonald,<sup>a</sup> T. Matt Letvenuk,<sup>a</sup> Christian E. Carello,<sup>a</sup> Michael Jennings,<sup>b</sup> Alan J. Lough,<sup>c</sup> James Britten,<sup>d</sup> Andreas Decken<sup>e</sup> and Kathryn E. Preuss<sup>a</sup>

Under aprotic conditions, the reaction of 4-amino-1,2-naphthoquinone with excess S<sub>2</sub>Cl<sub>2</sub> generates 4,5-dioxo-naphtho[1,2-*d*][1,2,3]dithiazol-2-ium chloride in a typical Herz condensation. By contrast, prior literature reports an imine (NH) product, 4,5-dioxo-1*H*-naphtho[1,2-*d*][1,2,3]dithiazole, for the same reaction performed in acetic acid. Herein, the cation product is isolated with four different counter-anions (Cl<sup>-</sup>, GaCl<sub>4</sub><sup>-</sup>, FeCl<sub>4</sub><sup>-</sup> and OTf<sup>-</sup>). Reduction of the cation generates a neutral radical 1,2,3-dithiazolyl-*o*-naphthoquinone, with potential ligand properties. Further reduction generates a closed shell anion, isolated as a water-stable Li<sup>+</sup> complex and exhibiting *O,O*-bidentate chelation. The hydroxy (OH) isomer of the original imine (NH) product is reported, and this can be readily deprotonated and acylated (OAc). All species are structurally characterized. Solution redox behaviour and EPR are discussed where appropriate.

### Introduction

A quinone is a class of compound derived from the oxidation of an aromatic diol. In nature, as well as in industrial processes, the typical role of a quinone takes advantage of specific redox properties. The reversible reduction of a quinone occurs in two consecutive one-electron steps, first generating a paramagnetic anion, known as a semiquinone, then an aromatic dianion, known as a catecholate (Scheme 1). Since quinones and their derivatives can act as non-innocent ligands, readily coordinating to a variety of metal cations, their potential role in developing molecule-based materials is of particular interest. Strong, predictable exchange coupling between the magnetic moments of the semiquinone and metal ions can be exploited to develop materials with unique properties, such as metal-organic frameworks (MOFs) that exhibit activated conductivity and magnetic ordering<sup>1</sup> or microporous magnets with solvent-induced switching.<sup>2</sup> Access to multiple redox states and intra-molecular redox processes can generate “switchable” behaviour, such as so-called “valence tautomerism”.<sup>3</sup>

In our quest to design and develop novel radical ligands, we are exploring the ligand properties of paramagnetic thiazyl

building blocks.<sup>4</sup> Odd-electron thiazyl heterocycles tend to have large spin density on substituent-free S and N atoms, and thus readily engage in intermolecular interactions. These interactions can be employed as a supramolecular synthon,<sup>5,6</sup> as a means to phase transition behaviour,<sup>7</sup> or as a pathway for long-range magnetic ordering.<sup>8</sup> The possibility of designing ligands with both quinone and thiazyl functional groups is intriguing. To this end, we are exploring the properties of 1,2,3-dithiazolyl naphthoquinones.<sup>9</sup> Herein, we report the preparation, isolation, and extensive characterization of 1,2,3-dithiazolyl-*o*-naphthoquinone **1**, in its neutral radical, closed shell anion **1**<sup>-</sup>, and closed shell cation **1**<sup>+</sup> oxidation states. We also demonstrate modification of the anion to generate the protonated **2** and the acetylated **3** derivatives (Scheme 2).

### Results and Discussion

#### Synthesis

The action of excess sulfur monochloride on an aromatic primary amine, generating a 1,2,3-dithiazolium chloride, is known as the Herz reaction.<sup>10</sup> Although the mechanism of the Herz reaction has been a matter of debate for several decades, elegant work by Inamoto *et al.* helped elucidate key aspects of the condensation,<sup>11</sup> suggesting a 5*H*-1,2,3-dithiazole intermediate (Scheme 3). Prior to Inamoto's work, a 3*H*-1,2,3-dithiazole intermediate had been proposed<sup>12,13</sup> (Scheme 3), based in part on the reaction of sulfur monochloride and 4-amino-1,2-naphthoquinone (**H<sub>2</sub>N-NQ**), which is exactly the reaction that we report herein. Unlike most Herz reactions which proceed to completion yielding a cation chloride, it was shown that treating **H<sub>2</sub>N-NQ** with excess S<sub>2</sub>Cl<sub>2</sub> in acetic acid yields the 1*H*-naphtho[1,2-*d*][1,2,3]dithiazole-4,5-dione **4** (Scheme 3).<sup>12,13</sup> Gompper *et al.* report **4** (dark brown prisms;

<sup>a</sup> Department of Chemistry, University of Guelph, Guelph, Ontario, Canada, N1G 2W1. Fax: +1-519-766-1499; Tel: +1-519-824-4120; E-mail: kpreuss@uoguelph.ca

<sup>b</sup> Freelance Crystallography, 185 Chelsea Ave., London, ON, N6J 3J5 Canada.

<sup>c</sup> Department of Chemistry, University of Toronto, Toronto, ON M5S 3H6, Canada.

<sup>d</sup> Department of Chemistry, McMaster University, Hamilton, ON L8S 4M1, Canada.

<sup>e</sup> Department of Chemistry, University of New Brunswick, Fredericton, NB E3B 5A3, Canada.

Electronic Supplementary Information (ESI) available: a simulated EPR spectrum of **1** (Fig. S1); cyclic voltammetry (CV) data on **1** (Fig. S2) and **3** (Fig. S3); crystallographic details and CIFs for all reported structures. See DOI: 10.1039/x0xx00000x

mp = 250–252 °C, with a colour change to red at 190 °C<sup>12</sup> and Hope and Wiles corroborate the findings (dark red crystals; mp = 254 °C;  $\nu(\text{N-H}) = 3125$ ,  $\nu(\text{CO}) = 1590$  and  $1565 \text{ cm}^{-1}$ ).<sup>13</sup> Later, Mayer *et al.* reported the EPR spectroscopic observation of neutral radical **1** as part of series of Herz reactions on vinylogous amides,<sup>14</sup> and therein also claim that **4** results from the reaction of  $\text{S}_2\text{Cl}_2$  and  $\text{H}_2\text{N-NQ}$ , and that oxidization of the product generates the radical **1**. Interestingly, Mayer *et al.* also report observing an EPR signal associated with **1** as a transient species during the Herz condensation, consistent with similar findings that suggest the radical itself is generally an intermediate in a Herz reaction.<sup>15</sup>

In our hands, using dry, aprotic solvent under inert atmosphere, **4** is *not* observed as the product of the Herz reaction of  $\text{H}_2\text{N-NQ}$  and  $\text{S}_2\text{Cl}_2$ . Instead, 4,5-dioxo-naphtho[1,2-*d*][1,2,3]dithiazol-2-ium chloride [**1**<sup>+</sup>][Cl<sup>-</sup>], which is the product expected from a conventional Herz reaction, is recovered (Scheme 2). Although the crude product of the reaction is rather impure, which is typical of such ring closures,<sup>16</sup> the identity of [**1**<sup>+</sup>][Cl<sup>-</sup>] and absence of **4** can be easily deduced. There are no peaks in the IR spectrum of the crude product that can be reasonably assigned as a  $\nu(\text{N-H})$  stretch. Anion metathesis successfully generates other cation salts in moderate to high yields: the triflate [**1**<sup>+</sup>][OTf<sup>-</sup>], the tetrachlorogallate [**1**<sup>+</sup>][GaCl<sub>4</sub><sup>-</sup>], and the tetrachloroferrate [**1**<sup>+</sup>][FeCl<sub>4</sub><sup>-</sup>] are reported herein. Furthermore, a single red crystal recovered from the crude red product was determined to be [**1**<sup>+</sup>][Cl<sup>-</sup>]. Finally, *reduction* generates the dark purple neutral radical species **1** in reasonable yield.

During the sublimation of purple radical **1** (190 °C;  $10^{-2}$  Torr), we consistently isolated a small number of red crystals from the bulk product. These red crystals are the first component to sublime and can be sublimed exclusively if a lower temperature is maintained (150 °C;  $10^{-2}$  Torr). In addition, we noted the unusually acute air-sensitivity of radical species **1**, rapidly turning from dark purple to red upon even the slightest exposure to the atmosphere. Interestingly, we have determined the red decomposition product to be **2**, which is related to **1** by reduction and protonation, and is the OH isomer of the NH imine **4**. The identity of **2** has been determined definitively (mp = 242–244 °C) by structural analysis. IR spectroscopy confirms that **2** is protonated at an oxygen atom ( $\nu(\text{O-H}) = 3281 \text{ cm}^{-1}$ ), not at the nitrogen (no  $\nu(\text{N-H})$  stretch). Indeed, **2** can be prepared in reasonable yield by reacting **1** with water (Scheme 2).

To further probe the accessible redox states of **1**, and to explore the reactivity of **2**, we have prepared the lithium salt of the anion [**1**<sup>-</sup>][Li<sup>+</sup>] by deprotonating **2** with LiH. Although [**1**<sup>-</sup>][Li<sup>+</sup>] does not readily form single crystals, the monohydrate tetramer ([Li<sup>+</sup>][**1**<sup>-</sup>·H<sub>2</sub>O]<sub>4</sub>) crystallizes reproducibly from wet organic solvent.

The anion **1**<sup>-</sup> is capable of acting as a bidentate ligand, as observed in the structure of ([Li<sup>+</sup>][**1**<sup>-</sup>·H<sub>2</sub>O]<sub>4</sub>). Substitution at one of the two oxygen positions is also possible, as demonstrated by deprotonation and acylation of **2** to generate **3**.

## Crystal Structures

Single crystals representing all three oxidation states, **1**<sup>+</sup>, **1**, and **1**<sup>-</sup>, as well as species **2** and **3**, have been used for structural analysis. The molecular structures and crystal packing features are discussed here.

One of the most reliable structural indicators of oxidation state in a quinone is the length of the C=O bonds. This distance is expected to increase upon reduction to the semiquinone and again upon further reduction to the catecholate. The species presented herein provide an interesting example in which the closed shell anion **1**<sup>-</sup>, hydroxide **2** and acetate **3** all represent a semiquinone-type oxidation state, and the radical **1** represents an open shell quinone-type oxidation state with possible resonance contributors that ought to lengthen at least one of the two C=O bonds, as shown in Scheme 2. This, then, leaves the cation **1**<sup>+</sup>, which arguably represents a higher oxidation state than a quinone.

Single crystal X-ray structures of [**1**<sup>+</sup>][Cl<sup>-</sup>], [**1**<sup>+</sup>][OTf<sup>-</sup>], [**1**<sup>+</sup>][GaCl<sub>4</sub><sup>-</sup>] and [**1**<sup>+</sup>][FeCl<sub>4</sub><sup>-</sup>] reveal essentially the same structural features for the closed shell cation **1**<sup>+</sup>, as shown in Figure 1. The C=O bond distances observed in [**1**<sup>+</sup>][Cl<sup>-</sup>] (1.221(6) and 1.227(5) Å) are, in fact, typical for a crystalline benzoquinone species,<sup>17</sup> however most of those observed in the triflate, tetrachlorogallate and tetrachloroferrate are markedly shorter (e.g., 1.205(3) and 1.209(3) Å in [**1**<sup>+</sup>][FeCl<sub>4</sub><sup>-</sup>]), as might be predicted for this oxidation state. These bond distances are presented for comparison, along with other relevant crystallographic data, in Table 1.

Discussion of the C=O bond distances observed in the crystal structure of **1** is complicated by the fact that there are two crystallographically unique molecules in the asymmetric unit, each participating in the formation of a pancake-bonded  $\pi$ -dimer, often characterized by a short sulphur-sulphur contact (3.113(1) Å; Figure 2). This dimerization should decrease the contribution from the oxygen-centred radical resonance contributor and promote more quinone-like C=O bond lengths. In fact, although the observed bond lengths are comparable to those in other quinone species, the C8-O1 distance in both molecules (1.215(2) and 1.2186(19) Å) is shorter than the C9-O2 distance (1.2310(19) and 1.229(2) Å). This suggests that, even in the dimerized species, there is still an observable influence from both radical resonance contributors.

Anion **1**<sup>-</sup> has been crystallized as the hydrated tetramer of the lithium salt, ([Li<sup>+</sup>][**1**<sup>-</sup>·H<sub>2</sub>O]<sub>4</sub>). In the solid-state structure, the tetramer is located at a centre of inversion such that there are, in fact, only two crystallographically unique anions, lithium cations, and water molecules. As illustrated in Figure 3a, the lithium cations are coordinated to the oxygen atoms of the anions. Li1 occupies a distorted square pyramidal site and is chelated by both crystallographically unique anions. Li2 occupies a roughly tetrahedral site, including coordination to the two water molecules. The carbon-oxygen bond distances in the tetramer are significantly longer than those observed for the cation and neutral oxidation state of the dione. Of the two C-O bonds, the C8-O1 distance is predictably shorter (1.264(7)

and 1.259(7) Å) than the C9-O2 distance (1.305(8) and 1.307(7) Å). These distances are roughly in line with those observed in coordination complexes of other semiquinone species (average ca. 1.28 Å).<sup>18</sup>

Alternatively, the semiquinone oxidation state can be structurally represented by hydroxide **2** and acetate ester **3**, shown in Figures 3b and 3c, respectively. In both cases, the R group (R = H, Ac) is bonded at the O2 oxygen atom. In the solid state, **2** exists as H-bonded pairs (O2-H2 bond, 0.92(5) Å; O1...H2 contact, 1.86(5) Å), reminiscent of the pairwise H-bonded carboxylic acid supramolecular synthon.<sup>19</sup> The carbon-oxygen distances are predictably shorter for the nominally double bond C8-O1 (1.241(4) Å for **2**; 1.237(2) Å for **3**) than for the single bond C9-O2 (1.347(5) Å for **2**; 1.391(2) Å for **3**) and there is a greater difference between the two bond distances than that observed in  $[(Li^+)[1] \cdot H_2O)_4$ . This reflects a contribution from resonance structures that might serve to delocalize the negative charge in the tetramer, and the lack of such a feature in **2** and **3**.

As discussed in the computational analysis section (*vide infra*), the singly occupied molecular orbital (SOMO) of **1** is a  $\pi^*$  orbital that is anti-bonding with respect to the sulphur-sulphur bond. Accordingly, the S1-S2 distance is expected to increase upon reduction from  $1^+$  to **1**. Indeed, an increase in length is observed, with S1-S2 bond distances measuring approximately 2.02, 2.06, and 2.09 Å respectively. Again, it should be noted that the bond distances quoted for **1** are in fact for the dimerized species.

For thiazyl species, particularly those containing an S-S bond, electrostatic intermolecular interactions in the solid state are frequently a significant factor determining the crystal packing. An interaction of the type  $S_{O_1}^{O_2} \dots X_{O_1}^{O_2}$  is often observed in the structures of thiazyl cations and neutral radicals alike.<sup>5,16,20</sup> In closed shell 1,2,3-dithiazolium cation chlorides,<sup>21</sup> hexafluorophosphates,<sup>22</sup> hexafluoroantimonates,<sup>23</sup> and perchlorates,<sup>24</sup> it is not uncommon to find the Cl<sup>-</sup> anion, or one of the Cl, F or O atoms of the compound anion, located roughly equidistant from the two sulphur atoms at a distance of ca. 3 Å, and approximately in the plane of the thiazyl ring. This scenario is representative of the S1...Cl1 and S2...Cl1 contacts found in the structure of  $[1^+][Cl^-]$ , and is clearly illustrated in Figure 1. By contrast, the in-plane S1...O3 and S2...O3 contacts in  $[1^+][OTf^-]$  are significantly shorter (ca. 2.7 Å), whereas in  $[1^+][FeCl_4^-]$  the S...Cl contacts are longer (ca. 3.3 Å) and slightly out-of-plane. The large range in contact distance ( $\pm 0.3$  Å) is not uncommon. Thiazyl cation triflates often have short sulphur-oxygen contacts (ca. 2.8 Å)<sup>25</sup> and tetrachlorogallates often have long sulphur-chlorine contacts (ca. 3.4 Å).<sup>26</sup> In our tetrachlorogallate,  $[1^+][GaCl_4^-]$ , there is only one short S...Cl in-plane contact at ca. 3.2 Å. Values for these and all other intermolecular contacts discussed below are listed in Table 2.

The crystal packing of the cation  $1^+$  salts is rather complex. Each of the species is subject to a different set of close contacts in the solid state. The packing of  $[1^+][Cl^-]$ , shown in Figure 4, includes close lateral contacts between O1 and neighbouring N1 and S2 atoms. There are also vertical contacts (along [010]) between chloride ions and the quinone carbon

atoms (C8, C9, C10) as well as between O1 and both sulphur atoms of the nearest neighbour molecules.

The tetrachlorogallate  $[1^+][GaCl_4^-]$  crystal packing is dominated by a T-shaped, or “edge-to-face”, interaction between O2 and the thiazyl ring of a neighbouring molecule, as illustrated in Figure 5. These interactions define arrays propagating in [010]. The tetrachlorogallate anions pack among the cation arrays with close contacts from Cl1, Cl2 and Cl4 to multiple neighbouring  $1^+$  sulphur atoms. As discussed in the computational analysis section (*vide infra*), significant positive charge density is located at the sulphur atoms. Thus electrostatic contacts between the tetrachlorogallate and, to a lesser extent, the oxygen atoms of neighbouring  $1^+$  cations, is apparent in the crystal packing.

The crystal packing of  $[1^+][FeCl_4^-]$  is quite complex with a large number of intermolecular close contacts. The dominant feature of the packing motif involves lateral N1...S2 contacts between two neighbouring cations that are related by inversion. The O2 atom of a third neighbouring cation is in close contact with these N1 and S2 atoms, forming a roughly equilateral triangle, as illustrated in Figure 6a. The tetrachloroferrate anions pack among the cation arrays forming multiple close contacts with nearest neighbours. The contacts from all nearest neighbour anions to a single cation are shown in Figure 6b.

An edge-to-face interaction between neighbouring cations, similar to that observed in the structure of  $[1^+][GaCl_4^-]$ , dominates the crystal packing of  $[1^+][OTf^-]$ . In this case, however, O1 forms close contacts with C8 and C9 of a neighbouring cation, which places O2 in proximity of the neighbouring S1 atom, as illustrated in Figure 7. The result is an array propagating in [010]. The triflate anions are located among the cations such that multiple short contacts are present.

Although the neutral species **1** has no formal charges, the importance of electrostatic interactions is still evident in the crystal packing. Apart from the short S...S contact that characterizes the formation of pancake-bonded  $\pi$ -dimers, there are a number of close lateral S...O contacts, presumably electrostatic in nature, between the dimers (Figure 8). The short intermolecular contacts serve to arrange the molecules in what appear to be sheets, or layers, separated by roughly 3.1 Å.

The crystal packing of neutral species **2** is primarily defined by the hydrogen bonding between pairs of molecules, shown in Figure 3. These H-bonded pairs are then arranged in a herring-bone motif with only one close contact worthy of note, between S1 and S2 of neighbouring molecules (ca. 3.5 Å). Similarly, neutral species **3** exhibits only one significant set of close contacts that direct its crystal packing: atom O1 occupies a position in-plane and roughly equidistant with both atoms of a neighbouring S1-S2 bond.

### Computational Analysis

The highest occupied molecular orbitals (HOMOs) of geometry optimized  $1^+$ , **1**, and **2** are illustrated in Figure 9 (B3LYP/6-

31G(d,p)) along with the singly occupied molecular orbital (SOMO) of **1** (uB3LYP/6-31G(d,p)).<sup>27</sup> As anticipated, the HOMO of semiquinone-like **1**<sup>-</sup> and the SOMO of quinone-like **1** are similar  $\pi^*$  orbitals, with large orbital coefficients on the S and N heteroatoms, as well as on one of the O atoms and the C atoms in between. Moreover, the spin density map of radical **1** shows large  $\alpha$  spin density (blue) at these atoms, in good agreement with the anticipated resonance contributors. The HOMO of semiquinone-like **2** is also similar to the HOMO of **1**<sup>-</sup>, with slightly more delocalization onto remote C atoms. By contrast, the HOMO of **1**<sup>+</sup>, which is nominally a higher oxidation state than a quinone, is quite different from the others and has predominantly  $\sigma$  character.

Calculated Mulliken charge densities are illustrated for **1**<sup>+</sup>, **1**<sup>-</sup>, and **2** in Figure 9, with negative charge density shown in red and positive charge density in green. Despite the differences in oxidation state and net charge, in all cases the N and O atoms bear significant negative charge density, suggesting potential coordination sites for metal cations, and the S atoms bear varying degrees of positive charge density.

### EPR Spectroscopy

The solution electron paramagnetic resonance (EPR) spectrum of neutral radical **1** in CH<sub>2</sub>Cl<sub>2</sub> was recorded at ambient temperature (Figure 10). The spectrum is dominated by a three-line 1:1:1 pattern, centred at  $g_{\text{iso}} = 2.0096$ , consistent with coupling to one <sup>14</sup>N nucleus. Further hyperfine splitting is also evident, consistent with coupling to multiple <sup>1</sup>H nuclei. Indeed, to achieve a reasonable simulation of the EPR spectrum, hyperfine coupling to four <sup>1</sup>H nuclei is necessary. The minimum set of parameters required to adequately simulate the EPR spectrum (correlation > 0.999; Figure S1 in the ESI) is:  $a_{\text{N}} = 2.934$  G,  $2 \times a_{\text{H}} = 0.386$  G,  $2 \times a_{\text{H}} = 0.299$  G, line width = 0.234 mT. These parameters are consistent with the literature, within reason (lit.  $g_{\text{iso}} = 2.0095$ ,  $a_{\text{N}} = 3.2$  G,  $4 \times a_{\text{H}} = 0.34$  G).<sup>14</sup> The features of the solution EPR spectrum are consistent with the calculated spin density surface (Figure 9), which predicts significant  $\alpha$  spin density at the N atom as well as a combination of  $\alpha$  and  $\beta$  spin density at all four hydrogen-bearing C atoms.

### Electrochemical Properties

Cyclic voltammetry (CV) performed on an acetonitrile solution of neutral radical **1** reveals two chemically reversible redox processes (Figure 11), one oxidative to the closed shell cation **1**<sup>+</sup> and one reductive to the closed shell anion **1**<sup>-</sup>. The oxidative process occurs at  $E_{1/2}^{1/1^+} = 0.80$  V ( $\Delta E_{\text{pp}} = 0.10$  V) and the reductive process occurs at  $E_{1/2}^{1^-/1} = -0.02$  V ( $\Delta E_{\text{pp}} = 0.10$  V). These results nicely mirror the three isolated oxidation states of **1** presented herein. There is also at least one irreversible reductive process  $E_{\text{red}}$  that is ill-defined in CH<sub>3</sub>CN. Using THF instead of CH<sub>3</sub>CN improves solubility of the negatively charged species and expands the solvent window in the reductive direction, allowing a more complete observation of the  $E_{\text{red}}$  processes (Figure S2 in the ESI). In THF,  $E_{1/2}^{1/1^+} = 0.79$  V ( $\Delta E_{\text{pp}} = 0.11$  V),  $E_{1/2}^{1^-/1} = -0.04$  V ( $\Delta E_{\text{pp}} = 0.12$  V),  $E_{\text{red}1} = -1.06$  V and  $E_{\text{red}2}$

= -1.77 V. Although the redox process at  $E_{\text{red}1}$  may represent reduction to a catecholate-like radical dianion oxidation state, it appears to be chemically unstable under the CV conditions.

CV was also performed on a CH<sub>3</sub>CN solution of acetate ester **3** (Figure S3 in the ESI). Interestingly, a reversible oxidative process at  $E_{1/2} = 0.81$  V ( $\Delta E_{\text{pp}} = 0.08$  V) is observed. Presumably, this represents a radical cation species that is stable under CV conditions. There is also one irreversible reductive process ( $E_{\text{red}} = -0.88$  V) within the solvent window.

## Experimental Section

### Synthesis

Reactions and manipulations were performed under argon atmosphere. Most organic solvents were dried and distilled under argon immediately prior to use: THF dried over Na/benzophenone, acetonitrile over P<sub>2</sub>O<sub>5</sub>, toluene over Na, and CH<sub>2</sub>Cl<sub>2</sub> over CaH<sub>2</sub>. Chlorobenzene was purchased anhydrous and used as received. Lithium hydride, sulphur monochloride, gallium trichloride, iron trichloride, and silver triflate were purchased from Sigma Aldrich and used as received. 4-Amino-1,2-naphthoquinone was prepared from 1,2-naphthoquinone (purchased from Acros Organics) following a literature method.<sup>28</sup> IR spectra were obtained as KBr pressed pellets on a Nicolet 4700 FTIR spectrometer at 4 cm<sup>-1</sup> resolution and ambient temperature. NMR spectra were collected on Bruker instruments (frequency as indicated) at the University of Guelph NMR Centre. EPR spectra were recorded on a Bruker EMX spectrometer at Guelph. Elemental analyses were performed by MHW Laboratories in Phoenix, AZ, USA. Mass spectrometry was performed by the WATSPEC facility, University of Waterloo, Waterloo, ON, Canada, using a JEOL HX110 double focusing mass spectrometer or by the McMaster Regional Centre for Mass Spectrometry (MRCMS), McMaster University, Hamilton, ON, Canada, using a Micromass GCT (GC-El/CI Time of Flight Mass Spectrometer).

**4,5-Dioxo-naphtho[1,2-d][1,2,3]dithiazol-2-ium chloride [1<sup>+</sup>][Cl<sup>-</sup>].** Excess S<sub>2</sub>Cl<sub>2</sub> (33.8 mL, 422 mmol) was added to a solution of 4-amino-1,2-naphthoquinone (12.1862 g, 70.3721 mmol) in 230 mL of CH<sub>3</sub>CN and the mixture was refluxed for 4 h. The resulting red slurry was filtered warm and the recovered red powder was washed with 2 × 50 mL of CH<sub>3</sub>CN and 1 × 40 mL of CH<sub>2</sub>Cl<sub>2</sub>, and then dried in vacuo. Crude yield 22.8105 g (>100%). The impure product was used in subsequent steps without further purification, as well as for analysis by IR and MS. A single crystal suitable for X-ray analysis was recovered from the crude solid. IR (KBr)  $\nu/\text{cm}^{-1}$ : 1704(m), 1679(vs), 1587(m), 1575(w), 1490(w), 1457(w), 1413(s), 1363(w), 1313(w), 1291(s), 1225(m), 1180(w), 1155(w), 1093(w), 1040(w), 993(w), 980(w), 912(m), 900(s), 848(s), 804(s), 784(m), 710(w), 697(m), 672(m), 650(w), 629(w), 557(w), 529(m), 515(w), 467(m). MS (EI+, r.t. 0.91 min.):  $m/z$  234.0 (M<sup>+</sup>, 56%), 206 (100, M-CO), 162 (18), 160 (10), 130 (26), 102 (12), 93 (4), 75 (4), 69 (2).

**4,5-Dioxo-naphtho[1,2-d][1,2,3]dithiazol-2-ium triflate [1<sup>+</sup>][OTf<sup>-</sup>].** A deficit of silver triflate (4.8016 g, 18.678 mmol)

was added to a red suspension of crude **[1<sup>+</sup>][Cl<sup>-</sup>]** (6.0012 g) in 75 mL of CH<sub>3</sub>CN. The reaction mixture was stirred at RT for 4 h, then filtered to remove a pale orange powder from the dark red solution. The solvent was removed from the filtrate to afford a dark purple solid. This solid was stirred for 1 h in 35 mL CH<sub>2</sub>Cl<sub>2</sub> resulting in the removal of a soluble purple portion, leaving **[1<sup>+</sup>][OTf<sup>-</sup>]** as a red-brown solid. Yield 1.8706 g (4.8796 mmol, 26%). Red needles suitable for X-ray analysis were grown by slow evaporation in vacuo of a 1:1 CH<sub>3</sub>CN:toluene solution at 0 °C. IR (KBr)  $\nu/\text{cm}^{-1}$ : 1716(w), 1688(s), 1653(w), 1636(w), 1591(m), 1560(w), 1542(w), 1508(w), 1496(w), 1466(w), 1415(s), 1371(w), 1279(vs, br), 1238(vs, br), 1225(w), 1183(m), 1172(w), 1155(m), 1099(w), 1030(w), 1022(s), 985(w), 913(m), 870(m), 818(w), 784(m), 761(w), 718(w), 698(w), 676(m), 636(s), 575(m), 533(w), 517(s), 463(w). Elem. Anal. Calcd. for C<sub>11</sub>H<sub>4</sub>F<sub>3</sub>NO<sub>5</sub>S<sub>3</sub>: C, 34.46; H, 1.05; N, 3.65%. Found: C, 34.38; H, 0.97; N, 3.42%. <sup>1</sup>H NMR  $\delta_{\text{H}}$ (400 MHz; CD<sub>3</sub>CN): 8.49 (1 H, br s), 8.30 (1 H, br s), 7.95 (2 H, br s).

**4,5-Dioxo-naphtho[1,2-d][1,2,3]dithiazol-2-ium tetrachlorogallate [1<sup>+</sup>][GaCl<sub>4</sub><sup>-</sup>]**. A deficit of gallium trichloride (1.3056 g, 7.4148 mmol) dissolved in 15 mL CH<sub>3</sub>CN was added over 20 min to a red suspension of crude **[1<sup>+</sup>][Cl<sup>-</sup>]** (2.5300 g) in 30 mL of CH<sub>3</sub>CN. After stirring for 1 h at RT, the reaction mixture was filtered to remove a grey solid from the dark red solution. The solvent was removed from the filtrate to afford a dark purple solid. This solid was washed with 3 × 20 mL CH<sub>2</sub>Cl<sub>2</sub> resulting in the removal of a soluble purple by-product, leaving **[1<sup>+</sup>][GaCl<sub>4</sub><sup>-</sup>]** as a red solid. Yield 2.8101 g (6.3033 mmol, 85%). Red needles suitable for X-ray analysis were grown by slow evaporation in vacuo of a 1:1 CH<sub>3</sub>CN:chlorobenzene solution at 0 °C. IR (KBr)  $\nu/\text{cm}^{-1}$ : 1689(s), 1620(w), 1589(m), 1577(w), 1541(w), 1494(w), 1458(w), 1410(s), 1387(w), 1325(w), 1283(s), 1235(s), 1204(s), 1099(w), 978(w), 914(m), 903(w), 870(m), 810(w), 781(s), 711(w), 698(w), 672(s), 653(w), 631(w), 528(m), 510(w), 459(w). Elem. Anal. Calcd. for C<sub>10</sub>H<sub>4</sub>Cl<sub>4</sub>GaNO<sub>2</sub>S<sub>2</sub>: C, 26.94; H, 0.90; N, 3.14%. Found: C, 27.12; H, 1.08; N, 2.93%. <sup>1</sup>H NMR  $\delta_{\text{H}}$ (400 MHz; CD<sub>3</sub>CN): 8.52 (1 H, br s), 8.31 (1 H, br s), 7.97 (2 H, br s).

**4,5-Dioxo-naphtho[1,2-d][1,2,3]dithiazol-2-ium tetrachloroferrate [1<sup>+</sup>][FeCl<sub>4</sub><sup>-</sup>]**. A deficit of iron trichloride (1.2028 g, 7.4155 mmol) dissolved in 40 mL CH<sub>3</sub>CN was added to a red suspension of crude **[1<sup>+</sup>][Cl<sup>-</sup>]** (2.5300 g) in 100 mL of CH<sub>3</sub>CN. After stirring for 1 h at RT, the reaction mixture was filtered to remove a grey solid from the dark red solution. The solvent was removed from the filtrate to afford a dark purple solid. This solid was washed with 3 × 20 mL CH<sub>2</sub>Cl<sub>2</sub> resulting in the removal of a soluble purple by-product, leaving **[1<sup>+</sup>][FeCl<sub>4</sub><sup>-</sup>]** as a red solid. Yield 2.5352 g (5.8693 mmol, 79%). Crystals suitable for X-ray analysis were grown by slow evaporation in vacuo of a 1:1 CH<sub>3</sub>CN:chlorobenzene solution at 0 °C. IR (KBr)  $\nu/\text{cm}^{-1}$ : 1687(vs), 1655(w), 1648(w), 1637(w), 1588(m), 1577(w), 1493(w), 1482(w), 1409(vs), 1386(w), 1326(w), 1308(w), 1286(s), 1237(s), 1205(s), 1198(w), 1164(w), 1097(m), 1051(w), 979(m), 912(m), 869(m), 811(m), 784(s), 783(w), 713(w), 698(w), 673(s), 653(w), 631(m), 526(w), 505(w), 493(w), 481(w), 459(w), 438(w), 417(w). Elem. Anal. Calcd. for C<sub>10</sub>H<sub>4</sub>Cl<sub>4</sub>FeNO<sub>2</sub>S<sub>2</sub>: C, 27.80; H, 0.93; N, 3.24%. Found: C, 28.00;

H, 1.06; N, 3.23%. <sup>1</sup>H NMR  $\delta_{\text{H}}$ (400 MHz; CD<sub>3</sub>CN): 8.64 (1 H, br s), 8.29 (1 H, br s), 8.00 (2 H, br s).

**Naphtho[1,2-d][1,2,3]dithiazolyl-4,5-dione 1**. CH<sub>3</sub>CN (60 mL) was added to a solid mixture of bis( $\eta^5$ -cyclopentadienyl)iron (0.6897 g, 3.707 mmol) and crude **[1<sup>+</sup>][Cl<sup>-</sup>]** (1.0000 g). The resulting slurry was stirred for 3 h, over which time it changed colour from red to purple. The solid was recovered by filtration and washed with 3 × 5 mL CH<sub>3</sub>CN to remove a dark red soluble by-product leaving the grey/purple solid **1**. Crude yield 0.5315 g (2.269 mmol, 61% as calculated from 4-amino-1,2-naphthoquinone). Sublimation under dynamic vacuum (10<sup>-2</sup> Torr), using a 3-stage gradient tube furnace (190, 115, 75 °C), produced purple-black crystalline blocks of **1**. Sublimation yield 0.2150 g (0.9177 mmol, 25%). IR (KBr)  $\nu/\text{cm}^{-1}$ : 1665 (m), 1649 (w), 1595 (m), 1561 (vs), 1540 (w), 1508 (w), 1490 (w), 1459 (w), 1407 (m), 1390 (w), 1380 (s), 1317 (w), 1260 (m), 1229 (m), 1159 (w), 1095 (w), 1041 (w), 987 (m), 897 (m), 876 (w), 808 (m), 775 (w), 715 (w), 694 (w), 661 (m), 650 (w), 628 (w), 536 (w), 480 (w), 463 (w), 431 (w). MS (EI+, r.t. 3.59 min.):  $m/z$  234.0 (M<sup>+</sup>, 56%), 206 (100, M-CO), 162 (17), 160 (9), 130 (22), 102 (9), 93 (3), 75 (2), 69 (1). Elem. Anal. Calcd. for C<sub>10</sub>H<sub>4</sub>NO<sub>2</sub>S<sub>2</sub>: C, 51.27; H, 1.72; N, 5.98%. Found: C, 51.24; H, 1.46; N, 6.07%.

**4-Hydroxy-naphtho[1,2-d][1,2,3]dithiazol-5-one 2**. CH<sub>3</sub>CN (150 mL) was added to a solid mixture of bis( $\eta^5$ -cyclopentadienyl)iron (1.7240 g, 9.2668 mmol) and crude **[1<sup>+</sup>][Cl<sup>-</sup>]** (2.5000 g). The resulting slurry was stirred at RT for 3 h to generate crude **1** as a solid precipitate. This solid was recovered by filtration and washed with 3 × 5 mL of CH<sub>3</sub>CN. It was then suspended in a mixture of 100 mL THF and 20 mL of deionized water and stirred, in air at RT, for 15 h, resulting in a red solution. The solvent was removed affording a red powder. Sublimation of this solid under dynamic vacuum (10<sup>-2</sup> Torr), using a 3-stage gradient tube furnace (150, 75, 50 °C), produced red microcrystalline needles of **2**. Yield 1.3560 g (5.7633 mmol, 62%); mp 242–244 °C. Crystals suitable for X-ray analysis were grown by recrystallization from CH<sub>2</sub>Cl<sub>2</sub>. IR (KBr)  $\nu/\text{cm}^{-1}$ : 3281(vs, br), 1619 (vs), 1594(vs), 1560(s), 1508(w), 1497(m), 1458(m), 1417(w), 1388(w), 1374(vs), 1334(m), 1308(w), 1265(s), 1213(m), 1160(w), 1137(w), 1097(w), 1045(w), 1016(m), 968(w), 893(w), 869(w), 795(s), 777(w), 769(m), 704(m), 664(s), 646(m), 620(m), 544(w), 533(w), 467(w), 454(w), 418(w). MS (EI+, r.t. 3.59 min.; 275 °C):  $m/z$  235.0 (M<sup>+</sup>, 100%), 207 (14, M-CO), 178 (7, M-C<sub>2</sub>H<sub>2</sub>O<sub>2</sub>), 149 (5), 130 (9), 103 (18), 102 (8), 76 (4), 57 (3). Elem. Anal. Calcd. for C<sub>10</sub>H<sub>5</sub>NO<sub>2</sub>S<sub>2</sub>: C, 51.05; H, 2.14; N, 5.95%. Found: C, 50.89; H, 2.40; N, 5.90%. <sup>1</sup>H NMR  $\delta_{\text{H}}$ (600 MHz; d<sup>6</sup>-DMSO): 10.65 (1 H, m), 8.39 (1 H, m), 8.18 (1 H, m), 7.80 (2H, m). <sup>13</sup>C NMR  $\delta_{\text{C}}$ (APT, 150 MHz; d<sup>6</sup>-DMSO): 173.2, 154.6, 143.0, 131.9, 131.3, 131.0, 129.3, 127.7, 126.0, 125.4.

**Lithium 5-oxo-naphtho[1,2-d][1,2,3]dithiazol-4-olate [Li<sup>+</sup>][1<sup>-</sup>]**. THF (100 mL) was added to a solid mixture of **2** (0.5000g, 2.123 mmol) and excess lithium hydride (0.0669 g, 8.42 mmol). The resulting slurry was stirred at RT for 15 h, over which time it changed colour from red to blue. The reaction mixture was filtered and the solid was washed with 3 × 5 mL THF until it appeared white. The blue filtrate and the solvent

wash fractions were combined and the solvent was removed *in vacuo* affording a blue-purple solid. The solid was suspended in 150 mL of ethyl acetate at gentle reflux for 30 min., recovered by filtration and dried overnight under dynamic vacuum ( $10^{-2}$  Torr, 170 °C) to afford blue-purple  $[\text{Li}^+][\mathbf{1}]$ . Yield 0.3617 g (1.50 mmol, 70%). IR (KBr)  $\nu/\text{cm}^{-1}$ : 1611(m), 1586(s), 1567(s), 1535(s), 1509(w), 1491(m), 1453(w), 1343(s), 1318(m), 1260(s), 1218(s), 1157(m), 1148(w), 1096(w), 1049(w), 1020(w), 902(w), 873(w), 794(s), 765(m), 710(w), 698(m), 669(w), 659(s), 646(w), 585(w), 558(m), 518(s), 509(w), 483(w), 465(m), 448(w), 431(w), 421(w), 414(w). MS (ESI-, r.t. 1.31 min., dry  $\text{CH}_3\text{CN}$ ):  $m/z$  353 ( $\text{M}+\text{Li}+\text{CH}_3\text{CN}+\text{O}(\text{CH}_2)_4\text{H}$ , 4%), 280 (18), 266 (34), 250 (70), 234.0 (100,  $\text{M}^+$ ), 194 (8,  $\text{M}-\text{C}_2\text{O}$ ), 145 (36), 101 (7). Elem. Anal. Calcd. for  $\text{C}_{10}\text{H}_4\text{LiNO}_2\text{S}_2$ : C, 49.79; H, 1.67; N, 5.81%. Found: C, 50.00; H, 1.80; N, 5.76%.  $^1\text{H}$  NMR  $\delta_{\text{H}}$ (400 MHz;  $d^6$ -DMSO): 8.19 (1 H, m), 8.03 (1 H, m), 7.65 (2 H, m).  $^{13}\text{C}$  NMR  $\delta_{\text{C}}$ (APT, 100 MHz;  $d^6$ -DMSO): 180.5, 157.0, 156.4, 130.3, 130.0, 129.7, 128.4, 126.6, 125.6, 124.6.

Purple blocks of monohydrate ( $[\text{Li}^+][\mathbf{1}]\cdot\text{H}_2\text{O}$ )<sub>4</sub> suitable for X-ray analysis were grown by slow evaporation of a 1:2 MeOH:toluene solution. IR (KBr)  $\nu/\text{cm}^{-1}$ : 3423(br), 1607(w), 1591(s), 1552(s), 1488(s), 1449(w), 1384(vs), 1360(w), 1316(w), 1266(s), 1223(m), 1159(m), 1054(w), 1016(m), 871(w), 796(s), 767(m), 700(m), 661(m), 646(w), 620(w), 556(m), 505(w).  $^1\text{H}$  NMR  $\delta_{\text{H}}$ (400 MHz;  $d^6$ -DMSO): 8.16 (1 H, m), 8.00 (1 H, m), 7.63 (2 H, m), 3.33(2 H, s).

**5-Oxo-naphtho[1,2-d][1,2,3]dithiazol-4-yl acetate 3.** Triethylamine (0.1452 g, 1.435 mmol) was added to a solution of **2** (0.2333 g, 0.9915 mmol) in dry THF (30 mL) and the mixture was stirred at RT for 15 min to generate a dark violet solution. Acetylchloride (0.1105 g, 1.408 mmol) was added and a colour change to orange was observed. The reaction mixture was stirred at RT for 2 h. An off-white solid was removed by filtration. The solvent was removed *in vacuo* from the remaining dark orange filtrate affording **3** as a red powder. Yield 0.1749 g (0.6307 mmol, 64%). Crystals suitable for X-ray analysis were grown by dynamic vacuum sublimation at 120 °C ( $10^{-2}$  Torr) and sent to the X-ray facility in the Department of Chemistry, University of New Brunswick, Fredericton, NB, Canada. IR (KBr)  $\nu/\text{cm}^{-1}$ : 3271(w), 1759(s), 1616(m), 1610(m), 1590(s), 1582(s), 1541(s), 1497(s), 1455(m), 1384(s), 1373(m), 1353(w), 1313(s), 1254(w), 1206(m), 1182(s), 1153(w), 1096(w), 1040(m), 1018(m), 964(w), 860(w), 815(s), 770(s), 727(w), 689(m), 672(m), 637(m), 618(w), 600(m), 584(m), 543(m), 486(w), 473(m), 419(w). MS (EI+, r.t. 1.88 min.):  $m/z$  277 ( $\text{M}^+$ , 8%), 235 (100,  $\text{M}-\text{OCCH}_3+\text{H}$ ), 207 (7,  $\text{M}-\text{COCCCH}_3+\text{H}$ ), 178 (3), 130 (5), 103 (5), 102 (3), 76 (1).  $^1\text{H}$  NMR  $\delta_{\text{H}}$ (300 MHz;  $d^6$ -DMSO): 8.44 (1 H, m), 8.16 (1 H, m) 7.87 (2 H, m), 2.37 (3 H, s, Me).

### Cyclic Voltammetry

Electrochemical measurements were performed at ambient temperature on solutions prepared using dry, degassed solvents with 0.1 M *n*Bu<sub>4</sub>NPF<sub>6</sub> electrolyte and ~2 mM analyte. Data were recorded on a BASi Epsilon-EC Bioanalytical

Systems, Inc. instrument, version 2.10.73\_USB, 2009, using platinum wire electrodes (working, reference, and counter), at scan rates of 100 and 200 mV/s. Where possible, the ferrocene/ferrocenium ( $\text{fc}/\text{fc}^+$ ) redox couple was used as an internal standard;  $E_{1/2}^{\text{fc}/\text{fc}^+} = +0.38$  V vs. SCE in MeCN;<sup>29</sup>  $E_{1/2}^{\text{fc}/\text{fc}^+} = +0.56$  V vs. SCE in THF.<sup>30</sup> Ferrocene was purchased from Aldrich and sublimed before use. In some instances, the  $\text{fc}/\text{fc}^+$  internal standard appeared to interfere with the analyte, so the quinone/semiquinone (Q/SQ) redox couple of chloranil (recrystallized from toluene) was employed as an alternative internal standard. We have determined that the chloranil  $E_{1/2}^{\text{Q/SQ}} = -0.01$  V and  $-0.04$  V vs SCE in MeCN and THF respectively, using  $\text{fc}/\text{fc}^+$  as the internal reference. All redox processes are reported versus SCE.

### Crystallography

**Crystal structure determination of  $[\mathbf{1}^+][\text{Cl}^-]$ :** A red, needle-shaped, single crystal was used for data collection at the McMaster Analytical X-ray Diffraction Facility (MAX), McMaster University, Hamilton, ON, Canada, on a Bruker Smart APEX-II CCD, radiation source MoK $\alpha$ , wavelength = 0.71073 Å.

**Crystal structure determination of  $[\mathbf{1}^+][\text{OTf}^-]$ :** A red, needle-shaped, single crystal was used for data collection at the McMaster Analytical X-ray Diffraction Facility (MAX), McMaster University, Hamilton, ON, Canada, on a Bruker Smart APEX-II CCD, radiation source MoK $\alpha$ , wavelength = 0.71073 Å.

**Crystal structure determination of  $[\mathbf{1}^+][\text{GaCl}_4^-]$ :** A purple-red, needle-shaped, single crystal was used for data collection at the McMaster Analytical X-ray Diffraction Facility (MAX), McMaster University, Hamilton, ON, Canada, on a Bruker Smart APEX-II CCD, radiation source MoK $\alpha$ , wavelength = 0.71073 Å.

**Crystal structure determination of  $[\mathbf{1}^+][\text{FeCl}_4^-]$ :** A purple, plate-shaped, single crystal was used for data collection at the Service Crystal Laboratory, University of Toronto, Toronto, ON, Canada, on a Bruker APEX-II area detector diffractometer, radiation source MoK $\alpha$ , wavelength = 0.71073 Å.

**Crystal structure determination of **1**:** A dark purple, block-shaped single crystal was used for data collection at the McMaster Analytical X-ray Diffraction Facility (MAX), McMaster University, Hamilton, ON, Canada, on a Bruker Smart APEX-II CCD, radiation source MoK $\alpha$ , wavelength = 0.71073 Å.

**Crystal structure determination of **2**:** A purple, needle-shaped, single crystal was used for data collection at the Service Crystal Laboratory, University of Toronto, Toronto, ON, Canada, on a Bruker APEX-II area detector diffractometer, radiation source MoK $\alpha$ , wavelength = 0.71073 Å. The H atom of the hydroxyl group was refined independently with an isotropic displacement parameter.

**Crystal structure determination of ( $[\text{Li}^+][\mathbf{1}]\cdot\text{H}_2\text{O}$ )<sub>4</sub>:** A purple, block-shaped, single crystal was used for data collection at the Service Crystal Laboratory, University of Toronto, Toronto, ON, Canada, on a Bruker APEX-II area

detector diffractometer, radiation source MoK $\alpha$ , wavelength = 0.71073 Å.

**Crystal structure determination of 3:** Data were collected at the X-ray facility in the Department of Chemistry, University of New Brunswick, Fredericton, NB, Canada. A single orange, rod-shaped crystal was coated with Paratone-N oil, mounted using a polyimide MicroMount and frozen in the cold nitrogen stream of the goniometer. A hemisphere of data was collected on a Bruker AXS P4/SMART 1000 diffractometer, radiation source MoK $\alpha$ , wavelength = 0.71073 Å, using  $\omega$  and  $\theta$  scans with a scan width of 0.3° and 30 s exposure times. The detector distance was 5 cm. The data were reduced (SAINT)<sup>31</sup> and corrected for absorption (SADABS).<sup>32</sup> The structure was solved by direct methods and refined by full-matrix least squares on  $F^2$ (SHELXL)<sup>33</sup>. All non-hydrogen atoms were refined using anisotropic displacement parameters. Hydrogen atoms were found in Fourier difference maps and refined using isotropic displacement parameters.

## Conclusions

Neutral radical naphtho[1,2-*d*][1,2,3]dithiazolyl-4,5-dione **1** provides a starting point to a family of related species and derivatives in higher and lower redox states. Illustrated in Scheme 2, **1** is prepared by reduction of the closed shell cation **1**<sup>+</sup>. The latter is generated as 4,5-dioxo-naphtho[1,2-*d*][1,2,3]dithiazol-2-ium chloride [**1**<sup>+</sup>][Cl<sup>-</sup>] from a Herz condensation of S<sub>2</sub>Cl<sub>2</sub> with 4-amino-1,2-naphthoquinone, and can be converted by anion metathesis to the triflate [**1**<sup>+</sup>][OTf<sup>-</sup>], the tetrachlorogallate [**1**<sup>+</sup>][GaCl<sub>4</sub><sup>-</sup>], and the tetrachloroferrate [**1**<sup>+</sup>][FeCl<sub>4</sub><sup>-</sup>]. Contrary to previous reports, we have not observed formation of the 3*H*-1,2,3-dithiazole species **4**, but instead observe a typical cation chloride [**1**<sup>+</sup>][Cl<sup>-</sup>] Herz product.

Neutral radical **1** is readily reduced and protonated by water to afford 4-hydroxy-naphtho[1,2-*d*][1,2,3]dithiazol-5-one **2**, a structural isomer of **4**. Deprotonation of **2** with lithium hydride generates the closed shell anion **1**<sup>-</sup> as lithium 5-oxo-naphtho[1,2-*d*][1,2,3]dithiazol-4-olate [Li<sup>+</sup>][**1**<sup>-</sup>]. Thus, compounds of all three oxidation states, **1**<sup>+</sup>, **1**, and **1**<sup>-</sup>, have been prepared and characterized. Anion **1**<sup>-</sup> acts as a chelating ligand, boding well for future use in the development of metal complexes with non-innocent thiazyl-quinone ligands.

Hydroxy species **2** is a potential gateway to the preparation of new species with substituents at the 4-position oxygen. In order to illustrate this, we have prepared 5-oxo-naphtho[1,2-*d*][1,2,3]dithiazol-4-yl acetate **3** by deprotonating **2** and treating it with acetylchloride. Acetate ester **3** exhibits a reversible oxidation process under CV conditions, suggesting that a stable radical cation may be accessible.

## Acknowledgements

K.E.P. thanks the following agencies for financial support: the Natural Sciences and Engineering Research Council (NSERC) of Canada for a Discovery Grant (DG), the Canada Foundation for Innovation (CFI) Leaders Opportunity Fund (LOF), the Ontario

Innovation Trust, the Government of Canada for a Tier II Canada Research Chair, and the University of Guelph for undergraduate research project support.

## Notes and references

- L. E. Darago, M. L. Aubrey, C. J. Yu, M. I. Gonzalez and J. R. Long, *J. Am. Chem. Soc.*, 2015, **137**, 15703.
- I.-R. Jeon, B. Negru, R. P. Van Duyne and T. D. Harris, *J. Am. Chem. Soc.*, 2015, **137**, 15699.
- R. M. Buchanan and C. G. Pierpont, *J. Am. Chem. Soc.*, 1980, **102**, 4951; S. Bin-Salamon, S. Brewer, S. Franzen, D. L. Feldheim, S. Lappi and D. A. Shultz, *J. Am. Chem. Soc.*, 2005, **127**, 5328; J. Tao, H. Maruyama and O. Sato, *J. Am. Chem. Soc.*, 2006, **128**, 1790; N. G. R. Hearn, J. L. Korčok, M. M. Paquette and K. E. Preuss, *Inorg. Chem.*, 2006, **45**, 8817; K. G. Alley, G. Poneti, J. B. Aitken, R. K. Hocking, B. Moubaraki, K. S. Murray, B. F. Abrahams, H. H. Harris, L. Sorace and C. Boskovic, *Inorg. Chem.*, 2012, **51**, 3944.
- K. E. Preuss, *Coord. Chem. Rev.*, 2015, **289-290**, 49.
- D. A. Haynes, *Cryst. Eng. Comm.*, 2011, **13**, 4793.
- K. E. Preuss, *Polyhedron*, 2014, **79**, 1.
- T. M. Barclay, A. W. Cordes, N. A. George, R. C. Haddon, M. E. Itkis, M. S. Mashuta, R. T. Oakley, G. W. Patenaude, R. W. Reed, J. F. Richardson and H. Zhang, *J. Am. Chem. Soc.*, 1998, **120**, 352; W. Fujita and K. Awaga, *Science*, 1999, **286**, 261; J. L. Brusso, O. P. Clements, R. C. Haddon, M. E. Itkis, A. A. Leitch, R. T. Oakley, R. W. Reed and J. F. Richardson, *J. Am. Chem. Soc.*, 2004, **126**, 8256; E. M. Fatila, R. A. Mayo, M. Rouzières, M. C. Jennings, P. Dechambenoit, D. V. Soldatov, C. Mathonière, R. Clérac, C. Coulon and K. E. Preuss, *Chem. Mater.*, 2015, **27**, 4023.
- A. J. Banister, N. Bricklebank, I. Lavender, J. M. Rawson, C. I. Gregory, B. K. Tanner, W. Clegg, M. R. J. Elsegood and F. Palacio, *Angew. Chem. Int. Ed.*, 1996, **35**, 2533; E. M. Fatila, R. Clérac, M. Rouzières, D. V. Soldatov, M. Jennings and K. E. Preuss, *J. Am. Chem. Soc.*, 2013, **135**, 13298; A. Mailman, S. M. Winter, J. W. Wong, C. M. Robertson, A. Assoud, P. A. Dube and R. T. Oakley, *J. Am. Chem. Soc.*, 2015, **137**, 1044.
- D. J. Sullivan, R. Clérac, M. Jennings, A. J. Lough and K. E. Preuss, *Chem. Commun.*, 2012, **48**, 10963.
- W. K. Warburton, *Chem. Rev.*, 1957, **57**, 1011; L. D. Huestis, M. L. Walsh and N. Hahn, *J. Org. Chem.*, 1965, **30**, 2763.
- Y. Inagaki, R. Okazaki and N. Inamoto, *Tetrahedron Lett.*, 1975, **16**, 4575; Y. Inagaki, R. Okazaki and N. Inamoto, *Bull. Chem. Soc. Jpn.*, 1979, **52**, 1998.
- R. Gompfer, H. Euchner and H. Kast, *Justus Liebigs Ann. Chem.*, 1964, **675**, 151.
- P. Hope and L. A. Wiles, *J. Chem. Soc. C*, 1967, 1642.
- R. Mayer, G. Domschke, S. Bleisch and A. Bartl, *Z. Chem.*, 1981, **21**, 324.
- S. R. Harrison, R. S. Pilkington and L. H. Sutcliffe, *J. Chem. Soc., Faraday Trans. 1*, 1984, **80**, 669.
- J. M. Rawson and G. D. McManus, *Coord. Chem. Rev.*, 1999, **189**, 135.
- D. R. Lide, ed., *CRC Handbook of Chemistry and Physics*, 72 edn., CRC Press, Inc., Boca Raton, 1991.
- D. Zirong, S. Bhattacharya, J. K. McCusker, P. M. Hagen, D. N. Hendrickson and C. G. Pierpont, *Inorg. Chem.*, 1992, **31**, 870; N. Shaikh, S. Goswami, A. Panja, X.-Y. Wang, S. Gao, R. J. Butcher and P. Banerjee, *Inorg. Chem.*, 2004, **43**, 5908.
- C. B. Aakeröy and K. R. Seddon, *Chem. Soc. Rev.*, 1993, 397.
- C. S. Clarke, D. A. Haynes, J. N. B. Smith, A. S. Batsanov, J. A. K. Howard, S. I. Pascu and J. M. Rawson, *Cryst. Eng. Comm.*, 2010, **12**, 172; M. B. Mills, A. G. Hollingshead, A. Maahs, D. V. Soldatov and K. E. Preuss, *CrystEngComm*, 2015, **17**, 7816.

- 21 T. M. Barclay, L. Beer, A. W. Cordes, R. T. Oakley, K. E. Preuss, N. J. Taylor and R. W. Reed, *Chem. Commun.*, 1999, 531; S. Rabe and U. Müller, *Z. Kristallogr. New Cryst. Struct.*, 1999, **214**, 68; K. Okamoto, T. Tanaka, W. Fujita, K. Awaga and T. Inabe, *Angew. Chem. Int. Ed.*, 2006, **45**, 4516.
- 22 T. M. Barclay, L. Beer, A. W. Cordes, R. T. Oakley, K. E. Preuss, R. W. Reed and N. J. Taylor, *Inorg. Chem.*, 2001, **40**, 2709.
- 23 L. Beer, R. T. Oakley, J. R. Mingie, K. E. Preuss, N. J. Taylor and A. W. Cordes, *J. Am. Chem. Soc.*, 2000, **122**, 7602.
- 24 T. M. Barclay, A. W. Cordes, R. T. Oakley, K. E. Preuss and R. W. Reed, *Chem. Mater.*, 1999, **11**, 164.
- 25 T. M. Barclay, L. Beer, A. W. Cordes, R. C. Haddon, M. I. Itkis, R. T. Oakley, K. E. Preuss and R. W. Reed, *J. Am. Chem. Soc.*, 1999, **121**, 6657; X. Yu, A. Mailman, P. A. Dube, A. Assoud and R. T. Oakley, *Chem. Commun.*, 2011, **47**, 4655.
- 26 L. Beer, A. W. Cordes, R. C. Haddon, M. E. Itkis, R. T. Oakley, R. W. Reed and C. M. Robertson, *Chem. Commun.*, 2002, 1872; M. Risto, A. Assoud, S. M. Winter, R. Oilunkaniemi, R. S. Laitinen and R. T. Oakley, *Inorg. Chem.*, 2008, **47**, 10100.
- 27 M. J. Frisch, G. W. Trucks, H. B. Schlegel, G. E. Scuseria, M. A. Robb, J. R. Cheeseman, G. Scalmani, V. Barone, B. Mennucci, G. A. Petersson, H. Nakatsuji, M. Caricato, X. Li, H. P. Hratchian, A. F. Izmaylov, J. Bloino, G. Zheng, J. L. Sonnenberg, M. Hada, M. Ehara, K. Toyota, R. Fukuda, J. Hasegawa, M. Ishida, T. Nakajima, Y. Honda, O. Kitao, H. Nakai, T. Vreven, J. J. A. Montgomery, J. E. Peralta, F. Ogliaro, M. Bearpark, J. J. Heyd, E. Brothers, K. N. Kudin, V. N. Staroverov, R. Kobayashi, J. Normand, K. Raghavachari, A. Rendell, J. C. Burant, S. S. Iyengar, J. Tomasi, M. Cossi, N. Rega, J. M. Millam, M. Klene, J. E. Knox, J. B. Cross, V. Bakken, C. Adamo, J. Jaramillo, R. Gomperts, R. E. Stratmann, O. Yazyev, A. J. Austin, R. Cammi, C. Pomelli, J. W. Ochterski, R. L. Martin, K. Morokuma, V. G. Zakrzewski, G. A. Voth, P. Salvador, J. J. Dannenberg, S. Dapprich, A. D. Daniels, O. Farkas, J. B. Foresman, J. V. Ortiz, J. Cioslowski and D. J. Fox, *Gaussian 09, Revision A.02* (2009) Gaussian Inc., Wallingford, CT.
- 28 L. F. Fieser and J. L. Hartwell, *J. Am. Chem. Soc.*, 1935, **57**, 1482.
- 29 R. T. Boéré, K. H. Mook and M. Parvez, *Z. Anorg. Allg. Chem.*, 1994, **620**, 1589.
- 30 N. G. Connelly and W. E. Geiger, *Chem. Rev.*, 1996, **96**, 877.
- 31 Bruker, *APEX2, SAINT*, 2007, Bruker AXS Inc., Madison, Wisconsin, USA.
- 32 Bruker, *SADABS*, 2001, Bruker AXS Inc., Madison, Wisconsin, USA.
- 33 G. M. Sheldrick, *Acta Crystallogr.*, 2008, **A64**, 112.

**Table 1** Crystallographic details including bond distances.

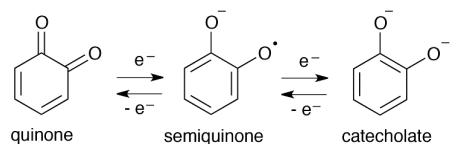
	[1 <sup>+</sup> ][Cl]	[1 <sup>+</sup> ][GaCl <sub>4</sub> ]	[1 <sup>+</sup> ][FeCl <sub>4</sub> ]	[1 <sup>+</sup> ][OTf]	1	([Li][1 <sup>+</sup> •H <sub>2</sub> O] <sub>4</sub> )	2	3
Formula	C <sub>10</sub> H <sub>4</sub> NO <sub>2</sub> S <sub>2</sub>	C <sub>10</sub> H <sub>4</sub> NO <sub>2</sub> S <sub>2</sub>	C <sub>10</sub> H <sub>4</sub> NO <sub>2</sub> S <sub>2</sub>	C <sub>11</sub> H <sub>4</sub> F <sub>3</sub> NO <sub>5</sub>	C <sub>10</sub> H <sub>4</sub> NO <sub>2</sub> S <sub>2</sub>	C <sub>40</sub> H <sub>24</sub> Li <sub>4</sub> N <sub>4</sub>	C <sub>10</sub> H <sub>5</sub> NO <sub>2</sub> S <sub>2</sub>	C <sub>12</sub> H <sub>7</sub> NO <sub>3</sub> S <sub>2</sub>
F.W.	269.71	445.78	431.91	383.33	234.26	1036.95	235.27	277.31
Crystal Setting	ortho-rhombic	monoclinic	monoclinic	ortho-rhombic	triclinic	monoclinic	monoclinic	monoclinic
Space Group	<i>Pnma</i>	<i>P2<sub>1</sub>/n</i>	<i>P2<sub>1</sub>/n</i>	<i>Pbca</i>	<i>P-1</i>	<i>P2<sub>1</sub>/c</i>	<i>P2<sub>1</sub>/n</i>	<i>P2<sub>1</sub>/n</i>
<i>a</i> / Å	19.620(5)	8.0862(15)	10.3004(3)	17.0537(17)	8.3156(16)	15.9640(12)	15.2462(14)	4.7207(5)
<i>b</i> / Å	5.8942(15)	9.4172(18)	11.1497(5)	6.4960(6)	10.872(2)	11.7083(15)	3.8351(2)	13.3232(13)
<i>c</i> / Å	8.422(2)	19.659(4)	13.8083(4)	25.224(3)	10.992(2)	11.632(2)	16.5627(14)	18.4301(18)
$\alpha$ (°)	90.00	90.00	90.00	90.00	61.995(3)	90.00	90.00	90.00
$\beta$ (°)	90.00	90.079(4)	110.605(2)	90.00	86.869(4)	101.590(8)	110.361(3)	92.977(2)
$\gamma$ (°)	90.00	90.00	90.00	90.00	85.509(4)	90.00	90.00	90.00
<i>V</i> / Å <sup>3</sup>	974.0(4)	1497.0(5)	1484.39(9)	2794.3(5)	874.5(3)	2129.8(5)	907.92(12)	1157.6(2)
<i>Z</i>	4	4	4	8	4	2	4	4
<i>T</i> / K	150(2)	150(2)	150(1)	150(2)	293(2)	150(1)	150(1)	198(1)
Reflections collected	9076	17035	9399	27184	5250	9127	5307	8030
Independent reflections	945	3088	3376	2462	6444	3590	2037	2604
<i>R</i> <sub>int</sub>	0.0651	0.0558	0.0475	0.0831	0.1313	0.0855	0.0767	0.0332
$\mu$ / mm <sup>-1</sup>	0.798	2.827	2.012	0.590	0.579	0.489	0.558	0.457
GOF	1.063	1.025	1.054	1.018	1.050	1.072	1.044	1.114
<i>R</i> <sub>1</sub> ( <i>I</i> > 2 $\sigma$ )	0.0373	0.0281	0.0363	0.0341	0.0355	0.0760	0.0586	0.0320
<i>wR</i> <sub>2</sub> ( <i>I</i> > 2 $\sigma$ )	0.0913	0.0529	0.0851	0.0694	0.0867	0.1705	0.1200	0.0751
<i>R</i> <sub>1</sub> (all data)	0.0529	0.0418	0.0541	0.0577	0.0441	0.1408	0.1280	0.0529
<i>wR</i> <sub>2</sub> (all data)	0.0988	0.0580	0.0945	0.0782	0.0925	0.2085	0.1505	0.0884
CCDC deposition #	1471457	1471458	1470545	1471459	1471642	1470546	1470547	1471460
Bond Distance (Å):					molecule <i>a</i> / molecule <i>b</i>	fragment <i>a</i> / fragment <i>b</i>		
O1 – C8	1.221(6)	1.204(3)	1.209(3)	1.217(3)	1.215(2) / 1.2186(19)	1.264(7) / 1.259(7)	1.241(4)	1.237(2)
O2 – C9	1.227(5)	1.201(3)	1.205(3)	1.200(3)	1.2310(19) / 1.229(2)	1.305(8) / 1.307(7)	1.347(5)	1.391(2)
N1 – C1	1.341(6)	1.330(3)	1.338(3)	1.336(3)	1.3265(19) / 1.3256(19)	1.319(8) / 1.326(8)	1.310(5)	1.306(2)
S1 – S2	2.0285(18)	2.0208(10)	2.0190(9)	2.0155(10)	2.0628(6) / 2.0680(7)	2.090(3) / 2.092(3)	2.1030(16)	2.0824(7)
Li1 – O1a						2.242(12)		
Li1 – O2a						2.023(12)		
Li1 – O2b						2.063(11)		
Li1 – O1b <sup>(iii)</sup>						2.009(12)		
Li1 – O2b <sup>(iii)</sup>						2.041(12)		
Li2 – O2b						1.946(12)		
Li2 – O1a <sup>(iii)</sup>						1.961(12)		
Li2 – O1W						1.903(11)		
Li2 – O2W						1.984(11)		
O2 – H2							0.92(5)	
O2 – C11								1.361(2)

Symmetry codes: (iii)  $-x, -y, 1 - z$ .

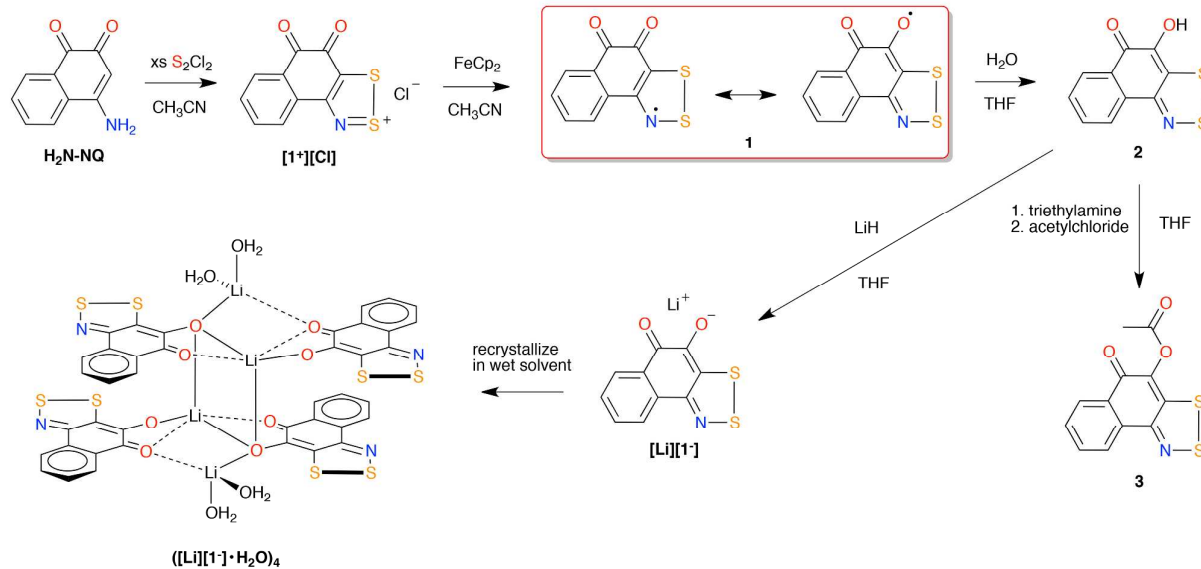
**Table 2** Solid state intermolecular contacts (Å)

	[1 <sup>+</sup> ][Cl]	[1 <sup>+</sup> ][GaCl <sub>4</sub> ]	[1 <sup>+</sup> ][FeCl <sub>4</sub> ]	[1 <sup>+</sup> ][OTf]	1	([Li][1 <sup>+</sup> •H <sub>2</sub> O] <sub>4</sub> )	2	3
Lateral cation-anion contacts	S1...Cl1	S2...Cl2	S1...Cl3 <sup>i</sup>	S1...O3				
	2.969(1)	3.167(2)	3.304(2)	2.770(3)				
	S2...Cl1		S2...Cl3 <sup>i</sup>	S2...O3				
	3.040(1)		3.287(2)	2.727(3)				
Other cation-anion contacts	C8...Cl1 <sup>vi</sup>	S2...Cl1 <sup>ix</sup>	S1...Cl2	S2...O4 <sup>xv</sup>				
	3.241(1)	3.303(2)	3.316(2)	2.934(3)				
	C9...Cl1 <sup>vi</sup>	C8 <sup>viii</sup> ...Cl2 <sup>ix</sup>	S1...Cl4 <sup>xiii</sup>	S2...O5 <sup>xv</sup>				
	3.043(1)	3.240(3)	3.316(2)	3.153(3)				
	C10...Cl1 <sup>vi</sup>	C9 <sup>viii</sup> ...Cl2 <sup>ix</sup>	C7...Cl4	S1...O3 <sup>xvi</sup>				
	3.180(1)	3.442(3)	3.367(3)	3.227(3)				
		S1 <sup>x</sup> ...Cl2 <sup>ix</sup>	C8...Cl4	S2...O3 <sup>xvi</sup>				
		3.548(2)	3.198(3)	3.095(3)				
		C10 <sup>x</sup> ...Cl4 <sup>ix</sup>	C9...Cl4	C1...O4 <sup>xvi</sup>				
		3.376(3)	3.152(3)	3.123(4)				
			C10...Cl4	C10...O4 <sup>xvi</sup>				
			3.389(3)	3.105(4)				
			C1...Cl1 <sup>xiii</sup>					
		3.409(3)						
		C9...Cl1 <sup>xiii</sup>						
		3.374(3)						
		C10...Cl1 <sup>xiii</sup>						
		3.222(3)						
Lateral contacts between thiazyl molecules	S2...O1 <sup>v</sup>		N1...S2 <sup>xi</sup>		S1a...O1b <sup>xvii</sup>			S1...O1 <sup>viii</sup>
	2.855(1)		3.127(2)		2.900(1)			2.866(2)
	N1...O1 <sup>v</sup>				S2a...O1b <sup>xvii</sup>			S2...O1 <sup>viii</sup>
	2.966(1)				2.894(1)			2.757(2)
					S2a...O2b <sup>xvii</sup>			
				3.019(1)				
				S1b...O1a				
				2.958(1)				
				S2b...O2a				
				2.766(1)				
Other contacts between thiazyl molecules	S1...O2 <sup>vii</sup>	O1 <sup>viii</sup> ...S2	N1...O2 <sup>xii</sup>	O1...C7 <sup>xiv</sup>	S1a...S1b <sup>xi</sup>	S1a...S1b <sup>xix</sup>	S1...S2 <sup>xviii</sup>	
	3.194(1)	3.307(3)	2.967(3)	3.119(4)	3.113(1)	3.579(3)	3.473(2)	
	S2...O2 <sup>vii</sup>	O2 <sup>viii</sup> ...S2	S2 <sup>xii</sup> ...O2 <sup>xii</sup>	O1...C8 <sup>xiv</sup>		S1a...C10 <sup>xix</sup>		
	3.267(1)	3.198(3)	3.195(3)	2.934(4)		3.563(6)		
		O2 <sup>viii</sup> ...N1		O1...C9 <sup>xiv</sup>		S2a...S2b <sup>xix</sup>		
		3.016(3)		2.914(4)		3.523(3)		
		O2 <sup>viii</sup> ...C1		O1...C10 <sup>xiv</sup>		S2a...N1b <sup>xix</sup>		
		2.988(3)		3.172(4)		3.265(6)		
		O2 <sup>viii</sup> ...C10		O2...S1 <sup>xiv</sup>		S2b...C2b <sup>xix</sup>		
		3.127(3)		3.002(3)		3.377(6)		
			O2...C10 <sup>xiv</sup>		S2b...C3b <sup>xix</sup>			
			3.126(4)		3.441(6)			
					S2b...C7b <sup>xix</sup>			
					3.495(6)			
Hydrogen bonding							O1...H2 <sup>iv</sup>	
							1.86(5)	

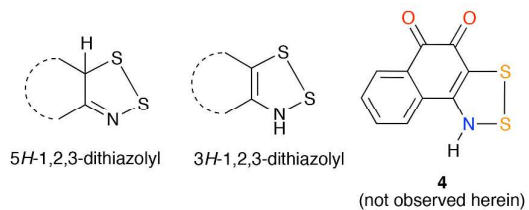
Symmetry codes: (i)  $x - \frac{1}{2}, \frac{1}{2} - y, z - \frac{1}{2}$ ; (ii)  $3 - x, 1 - y, 1 - z$ ; (iv)  $1 - x, 1 - y, 1 - z$ ; (v)  $x, y, z - 1$ ; (vi)  $3/2 - x, -y, z + \frac{1}{2}$ ; (vii)  $3/2 - x, -y, z - \frac{1}{2}$ ; (viii)  $x, y + \frac{1}{2}, 5/2 - z$ ; (viii)  $\frac{1}{2} - x, y - \frac{1}{2}, 3/2 - z$ ; (ix)  $3/2 - x, y - \frac{1}{2}, 3/2 - z$ ; (x)  $x, y - 1, z$ ; (xi)  $-x, -y, -z$ ; (xii)  $\frac{1}{2} - x, y - \frac{1}{2}, \frac{1}{2} - z$ ; (xiii)  $\frac{1}{2} - x, y + \frac{1}{2}, \frac{1}{2} - z$ ; (xiv)  $\frac{1}{2} - x, y - \frac{1}{2}, z$ ; (xv)  $-x, 2 - y, 1 - z$ ; (xvi)  $-x, 1 - y, 1 - z$ ; (xvii)  $x - 1, y, z - 1$ ; (xviii)  $\frac{1}{2} - x, y + \frac{1}{2}, 3/2 - z$ ; (xix)  $x, -y - \frac{1}{2}, z - \frac{1}{2}$ .



Scheme 1



Scheme 2



Scheme 3

---

[FIGURE 1]

**Figure 1.** Excerpts from the crystal structures showing the relative positions of the cation and anion components in a)  $[1^+][Cl^-]$ , b)  $[1^+][GaCl_4^-]$ , c)  $[1^+][FeCl_4^-]$ , and d)  $[1^+][OTf^-]$ ; anisotropic thermal ellipsoids illustrated at 50% probability; symmetry codes: (i)  $x - \frac{1}{2}, \frac{1}{2} - y, z - \frac{1}{2}$

---

{FIGURE 2}

**Figure 2.** Excerpt from the crystal structure of **1** showing the twisted cofacial dimerization mode; anisotropic thermal ellipsoids illustrated at 50% probability; symmetry codes: (ii)  $3 - x, 1 - y, 1 - z$

---

[FIGURE 3]

**Figure 3.** Excerpts from the crystal structures of a)  $([Li][1^+ \cdot H_2O])_n$ , b) **2**, highlighting the geometry of the intermolecular H-bonding interaction, and c) **3**; anisotropic thermal ellipsoids drawn at 50% probability; symmetry codes: (iii)  $-x, -y, 1 - z$ ; (iv)  $1 - x, 1 - y, 1 - z$

---

[FIGURE 4]

**Figure 4.** Excerpts from the crystal structure of  $[1^+][Cl]$  using dashed lines to illustrate close intermolecular contacts between neighbouring cations (red lines) and cation-anion contacts (green lines); a) view highlighting lateral contacts; b) view highlighting stacking interactions; symmetry codes: (v)  $x, y, z - 1$ ; (vi)  $3/2 - x, -y, z + 1/2$ ; (vii)  $3/2 - x, -y, z - 1/2$

---

[FIGURE 5]

**Figure 5.** Excerpt from the crystal structure of  $[1^+][GaCl_4]$  using dashed lines to illustrate close contacts between neighbouring cations (red lines) and cation-anion interactions (green lines); symmetry codes: (viii)  $1/2 - x, y - 1/2, 3/2 - z$ ; (ix)  $3/2 - x, y - 1/2, 3/2 - z$ ; (x)  $x, y - 1, z$

---

[FIGURE 8]

**Figure 8.** Excerpt from the crystal structure of radical **1** highlighting the packing motif defined by lateral contacts between dimers; symmetry codes: (ii)  $3 - x, 1 - y, 1 - z$ ; (xvii)  $x - 1, y, z - 1$

---

[FIGURE 9]

**Figure 9.** Line drawings, isosurfaces, and Mulliken charge density distribution (red = negative; green = positive) calculated using (u)B3LYP/6-31G(d,p) for neutral radical **1**, closed-shell cation  $1^+$ , closed-shell anion  $1^-$ , and **2**; for open-shell species, both the singly occupied molecular orbital (SOMO) and the total spin density distribution (alpha spin density = blue; beta spin density = green) are shown; for closed-shell species, the highest occupied molecular orbital (HOMO) is shown

---

[FIGURE 6]

**Figure 6.** Excerpts of the crystal structure of  $[1^+][FeCl_4]$  using dashed lines to illustrate close contacts between neighbouring cations (red lines) and cation-anion contacts (green lines); a) view highlighting cation-cation contacts and position of anions; b) view highlighting all nearest neighbour cation-anion contacts; symmetry codes: (i)  $x - 1/2, 1/2 - y, z - 1/2$ ; (xi)  $-x, -y, -z$ ; (xii)  $1/2 - x, y - 1/2, 1/2 - z$ ; (xiii)  $1/2 - x, y - 1/2, 1/2 - z$

---

[FIGURE 7]

**Figure 7.** Excerpt from the crystal structure of  $[1^+][OTf]$  highlighting the packing motif defined by edge-to-face interactions between cations (red lines) and the anion positions, with select cation-anion contacts (green lines); symmetry codes: (xiv)  $1/2 - x, y - 1/2, z$ ; (xv)  $-x, 2 - y, 1 - z$ ; (xvi)  $-x, 1 - y, 1 - z$

---



## Journal Name

### ARTICLE

---

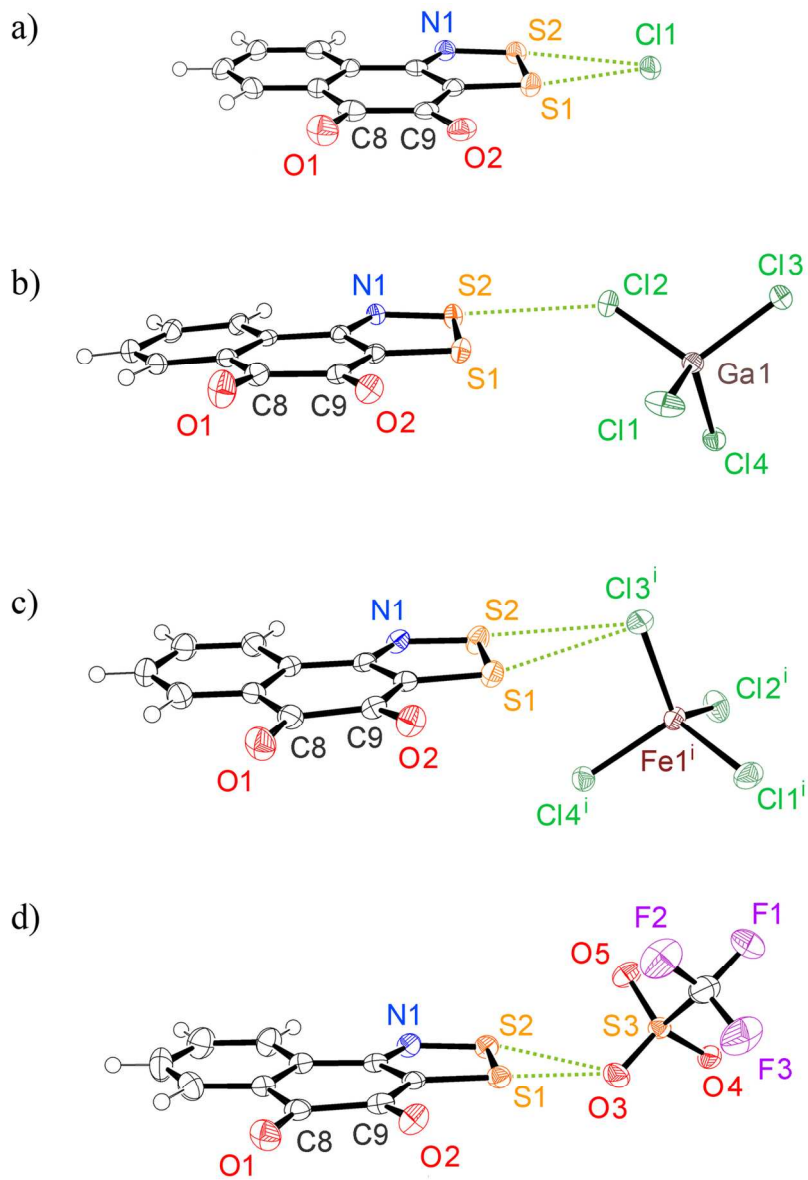
[FIGURE 10]

**Figure 10.** Diluted solution ( $\text{CH}_2\text{Cl}_2$ ) X-band EPR spectrum of **1** at ambient temperature

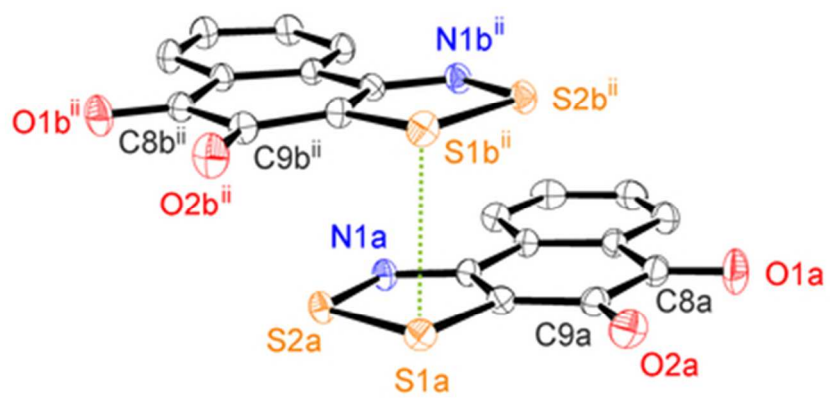
---

[FIGURE 11]

**Figure 11.** Cyclic voltammogram of **1** in  $\text{CH}_3\text{CN}$

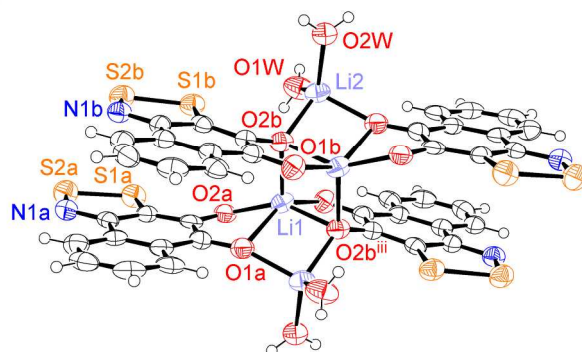


117x171mm (300 x 300 DPI)

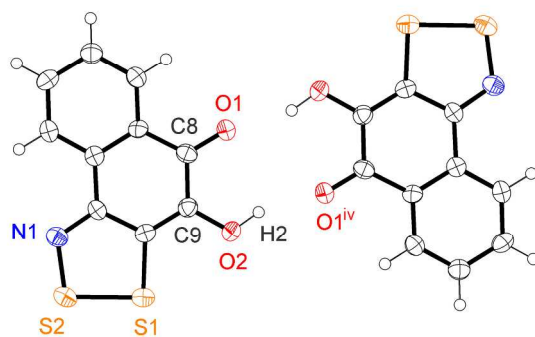


37x17mm (300 x 300 DPI)

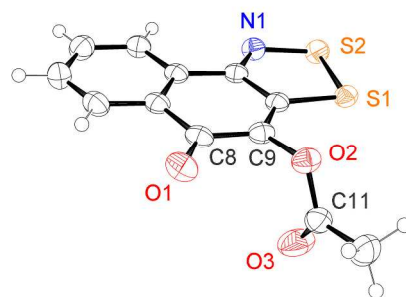
a)



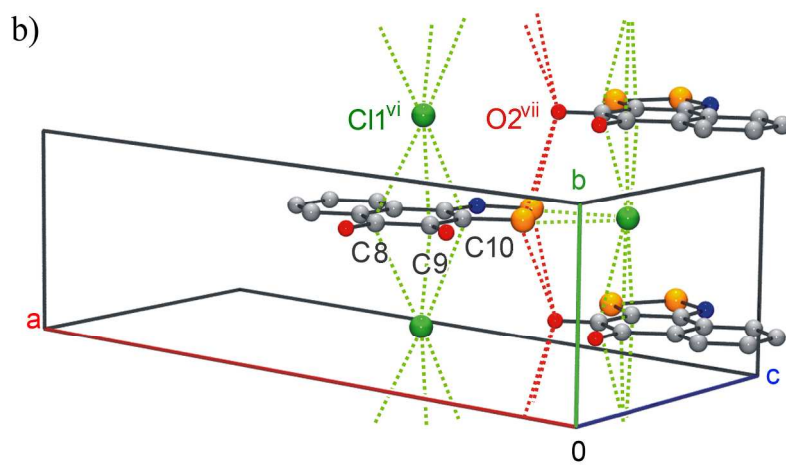
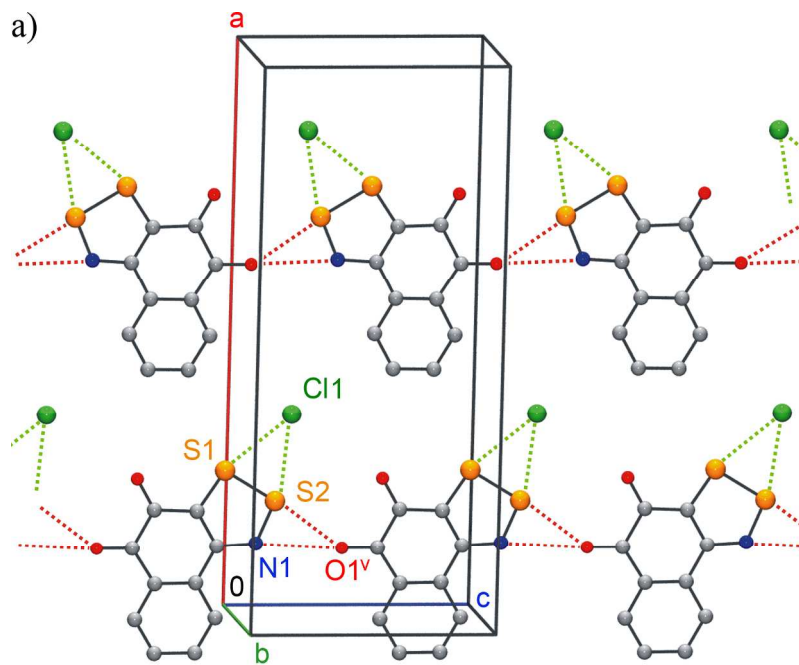
b)

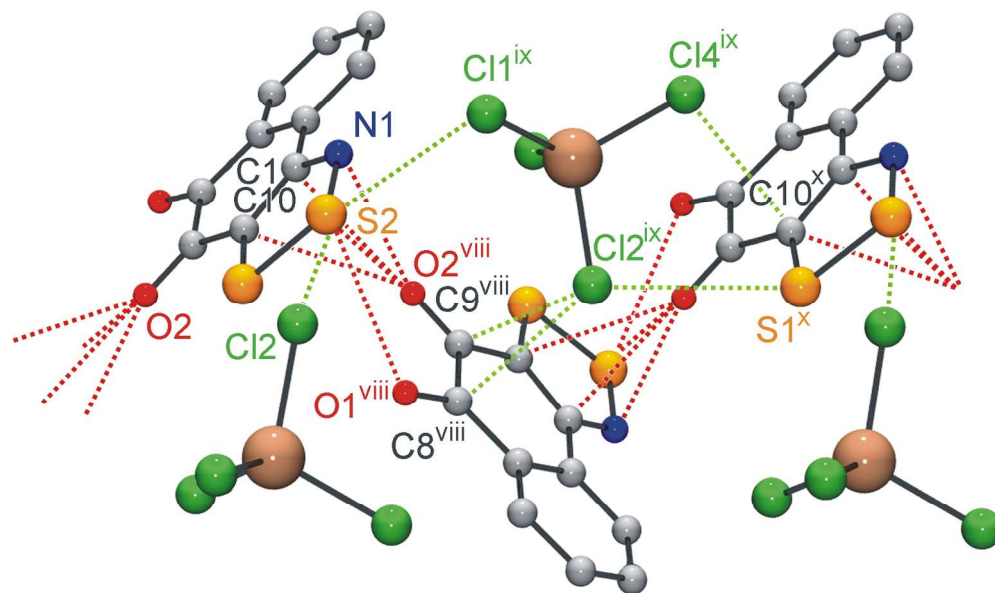


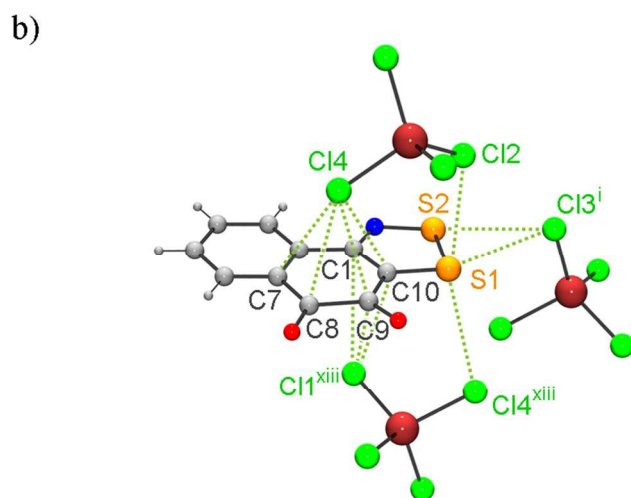
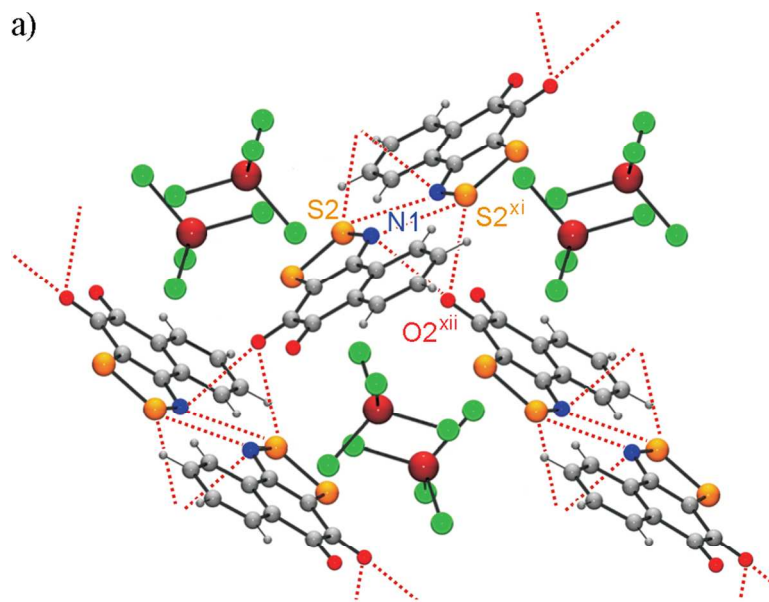
c)



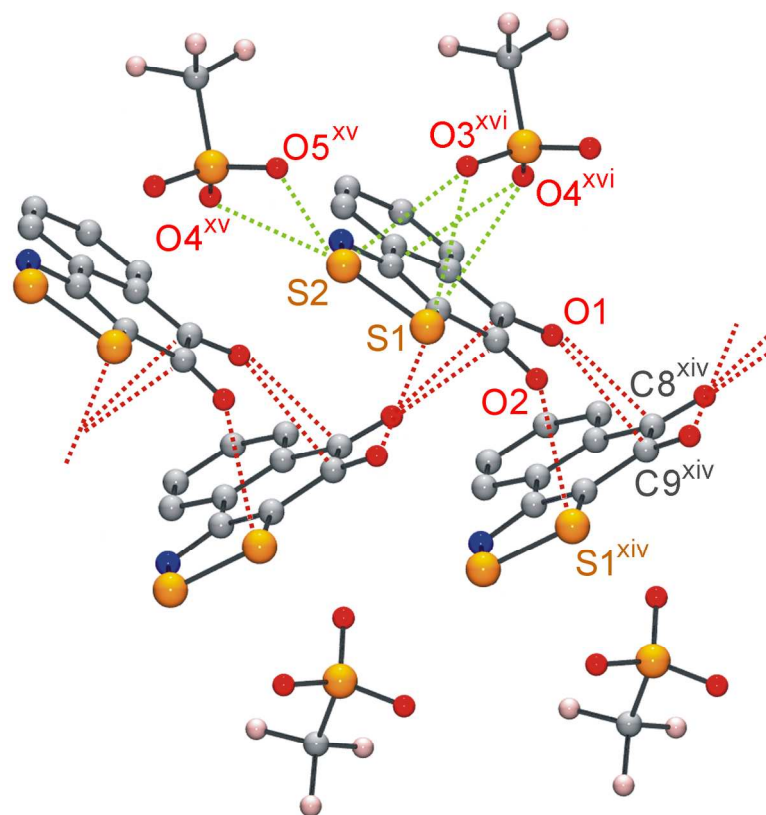
154x297mm (300 x 300 DPI)

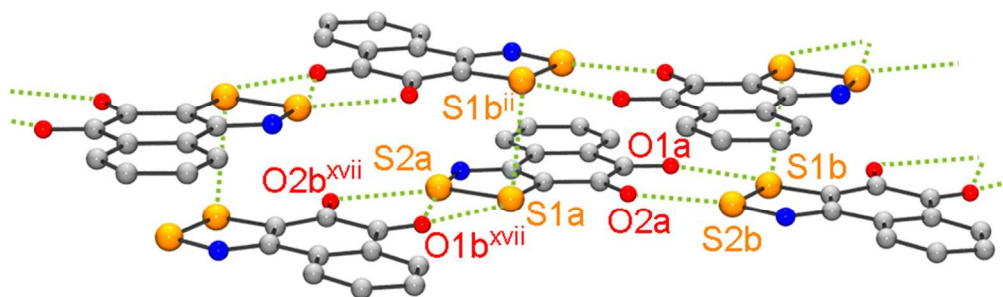




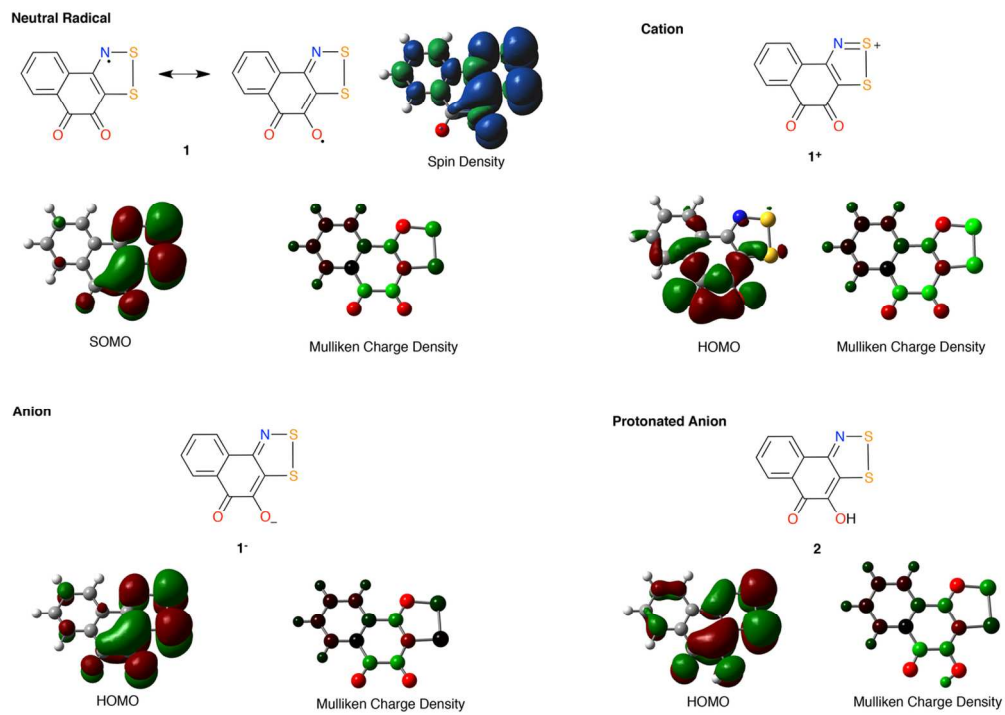


80x125mm (300 x 300 DPI)

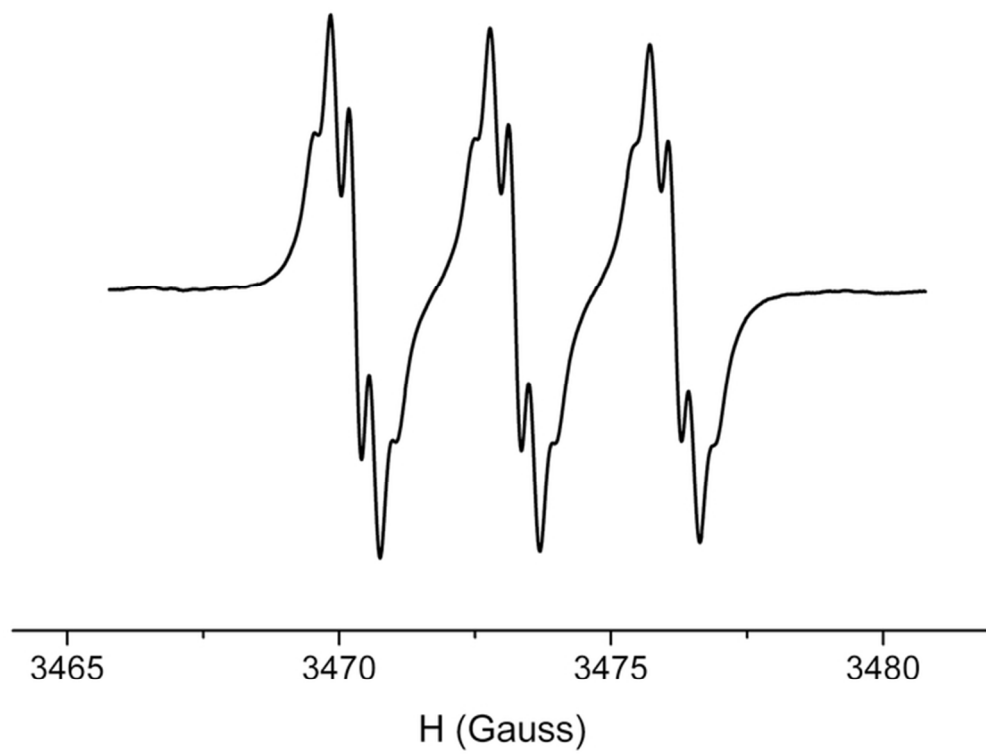




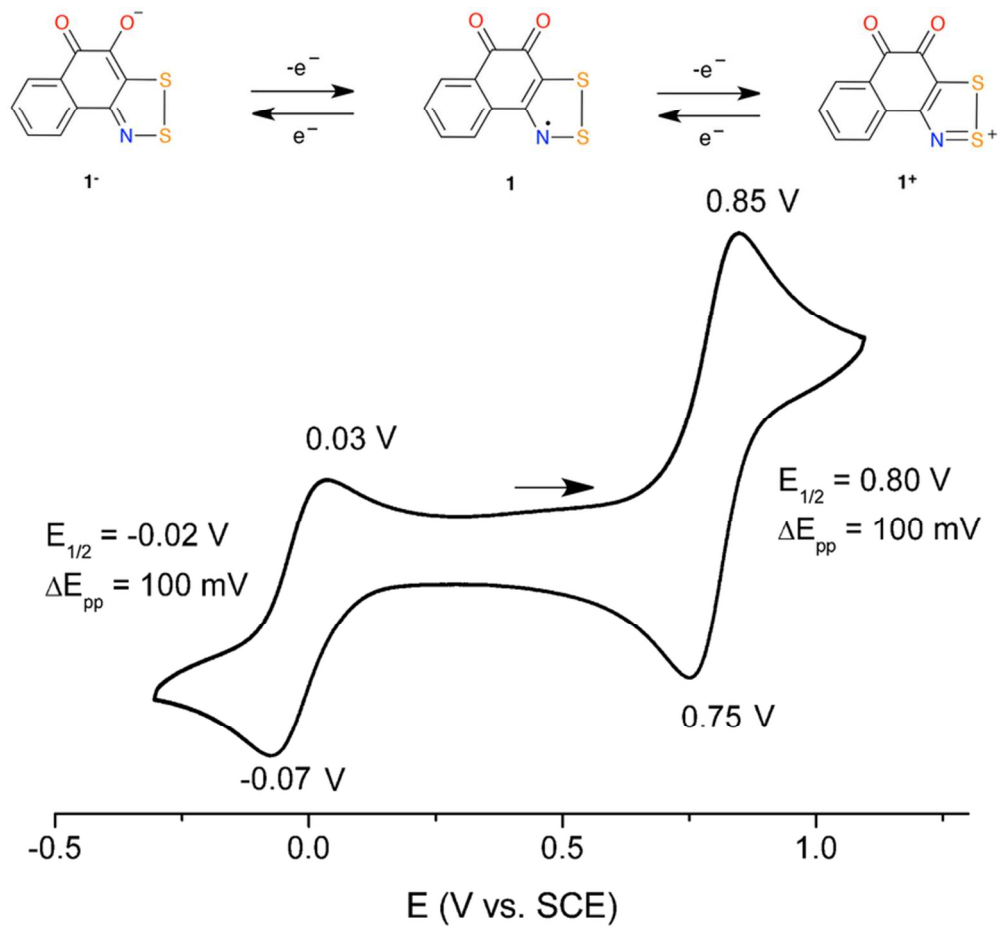
80x25mm (300 x 300 DPI)



121x87mm (300 x 300 DPI)



62x49mm (300 x 300 DPI)



73x68mm (300 x 300 DPI)